Journal of Alloys and Compounds 480 (2009) 857–862

Contents lists available at ScienceDirect

Journal of Alloys and Compounds

journal homepage: www.elsevier.com/locate/jallcom

An evaluation of the properties of As-cast U-rich U–Zr alloys

Chandrabhanu Basak[a,*], G.J. Prasad[a], H.S. Kamath[a], N. Prabhu[b]

[a] Metallic Fuels Division, Bhabha Atomic Research Center, Trombay, Mumbai 400 085, India
[b] Dept. of Met. Engg. and Mat. Sci., Indian Institute of Technology, Bombay, Powai, Mumbai 400 076, India

ARTICLE INFO

Article history:
Received 23 December 2008
Received in revised form 9 February 2009
Accepted 14 February 2009
Available online 4 March 2009

Keywords:
Uranium alloy
Microstructure
Dilatometry
X-ray diffraction

ABSTRACT

The present study involves evaluation of some basic properties of as-cast uranium rich U–Zr alloys, i.e. uranium alloys containing 2 wt%, 5 wt%, 7 wt% and 10 wt% zirconium. Microstructural evaluation, both optical and SEM, with hardness values are reported. Lattice parameter and densities are determined with XRD analysis. Thermal expansions are measured by dilatometry; also the phase transformation mechanism is proposed based on the microstructures, XRD analysis and dilatometric results. Quantification of the variation of different physical properties as a function of the Zr content is also presented here.

1. Introduction

The U–Zr binary alloy is an important subsystem of the U–Pu–Zr ternary alloy, which has been recognized as a promising metallic nuclear fuel in the fast breeder reactor. Also, U-rich U–Zr alloys are of interest because of their potential use in low power or research reactor, since Zr has a low thermal-neutron cross-section. Moreover, uranium alloyed with Zr has excellent corrosion resistance and dimensional stability during thermal cycling. These favorable properties have led to the development of uranium–zirconium fuel elements for reactor use and U-10 wt%Zr has already been irradiated in EBR-II, USA, in early 1985 [1]. Uranium alloys are always preferred in as-cast condition as reactor fuel since mechanical working can induce unwanted texture in it and subsequent irradiation induced growth.

Heat capacity and thermal diffusivity measurements are reported by Takahashi et al. for Zr-rich U–Zr alloys [2,3]. Only a few open literatures are available which report a systematic and comprehensive study on the influence of Zr concentration on the various physical properties of U-rich U–Zr alloys. Lagerberg [4] has reported the phase transformation behaviour in U-2 wt%Zr and recently the same is re-evaluated by Basak et al. [5]. Transformation behaviour on quenching of different U–Zr alloys is described by Hills et al. [6]. The elaborate work on U–Zr system could be found in the reports edited by Rough [7] and Bauer [8]. In both the reports a general discussion on the physical and metallurgical behaviour of U–Zr alloys is reported, mostly on quenching and ageing. Physical properties such as density, electrical resistivity, thermal conductivity, interdiffusion and different mechanical properties are also reported for the entire alloy range, with emphasis on the Zr-rich U–Zr alloys [2,7,8]. Some thermal expansion data are also reported for the alloys with Zr content more than 59 wt% [7,8]. However, it appears that while much work is reported on the Zr-rich U–Zr alloys regarding their physical properties, the same is not much available for U-rich alloys.

The present investigation deals mostly with the structure–property correlations in the U-rich U–Zr alloys with Zr concentration of 2 wt%, 5 wt%, 7 wt% and 10 wt%. The paper reports the as-cast microstructures and hardness values of U-rich U–Zr alloys. Variations in lattice parameters and densities, derived from the XRD analysis, are reported here as a function of Zr concentration. Dilatometric results are also presented here and equations of the thermal expansion are derived for these alloys. Also due inferences are drawn regarding the phase transformation behaviour of these alloys from the microstructures, XRD analysis and dilatometric results. Referring to the U-rich part of U–Zr phase diagram (Fig. 1), it is easy to find that the choice of the present alloy compositions encompasses the monotectoid point.

2. Experimental methods

Uranium slugs and crystal bar zirconium was obtained from the Atomic Fuels Division and Materials Processing Division of BARC respectively for making these alloys. All the U–Zr alloy samples were prepared in a high temperature vacuum induction furnace; both melting and solidification took place inside the yttria lined graphite crucible of 12.5 mm ID, 36 mm OD and 70 mm height. Furnace temperature was kept at 100 °C above the liquidus temperature of the respective alloy, with a holding time of 20 min. Typical weight of the alloy slugs was around 80 g. Standard CNO analysis shows presence of carbon, nitrogen and oxygen in these alloys. For

* Corresponding author. Tel.: +91 22 2559 0672.
E-mail address: cbbasak@barc.gov.in (C. Basak).

0925-8388/$ – see front matter © 2009 Elsevier B.V. All rights reserved.
doi:10.1016/j.jallcom.2009.02.077

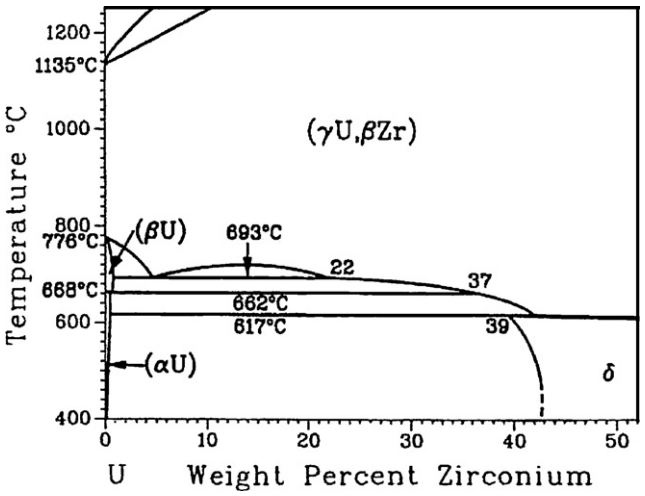

Fig. 1. U-rich part of the U–Zr phase diagram.

U-10 wt%Zr alloy, highest liquidus temperature among these alloys, the typical values of C, N and O are 450 ppm, 60 ppm and 580 ppm respectively. For other alloys these values are in general smaller. Other impurities are totaling to only 300 ppm as revealed by the Inductively Coupled Plasma-Atomic Emission Spectroscopic (ICP-AES) analysis. Analysis of Zr was also done by the ICP-AES. Results of the chemical analyses are presented in Table 1.

For dilatometric experiments the slugs were machined to 10 mm diameter and then cut into parallel-sided cylinder. LVDT based dilatometer was used with a heating rate of 1 °C/min under high purity argon atmosphere. For the metallographic and XRD analyses the alloy slugs were cut into disc of suitable thickness using slow speed SiC abrasive cut-off wheel. Standard metallographic techniques were adopted for grinding and polishing using cold setting resin mounts. For electro-etching a 5%H_3PO_4 aqueous solution was used with SS304 cathode, constant 2 V DC was applied for the etching. However, prior to the XRD analysis the samples were demounted and repolished. Cu-K_α radiation was used for XRD analysis with fixed slit optics and θ–θ goniometer. For the microhardness measurement diamond pyramid indentor was used with 200 g load and 15 s dwell time.

3. Results and discussion

3.1. Microstructure

As cast grain structure of uranium based alloys, being anisotropic in nature, are best revealed under polarized light. Fig. 2(a–d) show typical microstructures of U-rich U–Zr alloys under polarized light illumination. It is clear that the grains are irregular as that of pure uranium. However, with increase in Zr concentration the grain size is seen to be reduced. The variation in grain size with Zr content could be attributed to the cooling condition of the alloys. Alloy rich in Zr is having higher melting temperature, therefore, during cooling the initial rate of drop in temperature is more. In other word, higher initial temperature leads to higher rate of cooling primarily due to the radiative heat loss. So, the thermal undercooling is more predominated in Zr rich alloys leading to high rate of nucleation; which is later manifested as smaller grain size.

Bright field illumination reveals lamellar structure in 2 wt% and 5 wt%Zr alloys, however, optical microscopy was unable to resolve the lamellar structure in 7 wt% and 10 wt%Zr alloys. Scanning electron microscopy (SEM) was carried out for all the samples, as presented in Fig. 3(a–d). The secondary electron image was preferred over back scattered electron image since the former offers better resolution. While 3000× magnification is enough to resolve the lamellar structure in 2 wt% and 5 wt% alloy; the same can be observed in U-10 wt%Zr alloy only at 10,000× magnification with reduced spot size of the electron beam.

The reason why inter-lamellar spacing reduces as Zr content increases in the alloys can be explained by the role of Zr. During cooling the alloy rich in Zr undergoes all the decomposition reactions at relatively lower temperature than that predicted from the phase diagram; since, it is known that Zr tend to stabilize gamma phase [2,7,8]. Clearly, as Zr increases in the alloys the decomposition reactions (e.g. monotectoid and eutectoid) take place at relatively

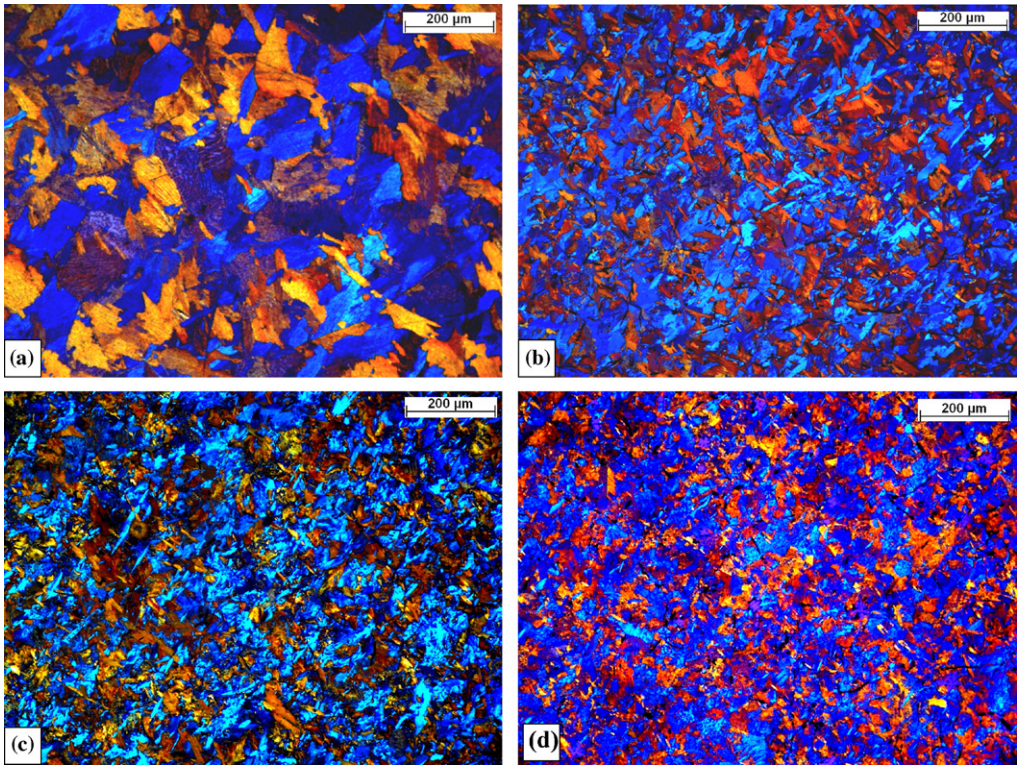

Fig. 2. Optical photomicrograph of as-cast U–Zr alloys under polarized light illumination; (a) U-2 wt%Zr, (a) U-5 wt%Zr, (c) U-7 wt%Zr and (d) U-10 wt%Zr. Note the irregular grain structure with reducing grain size with increasing Zr content.

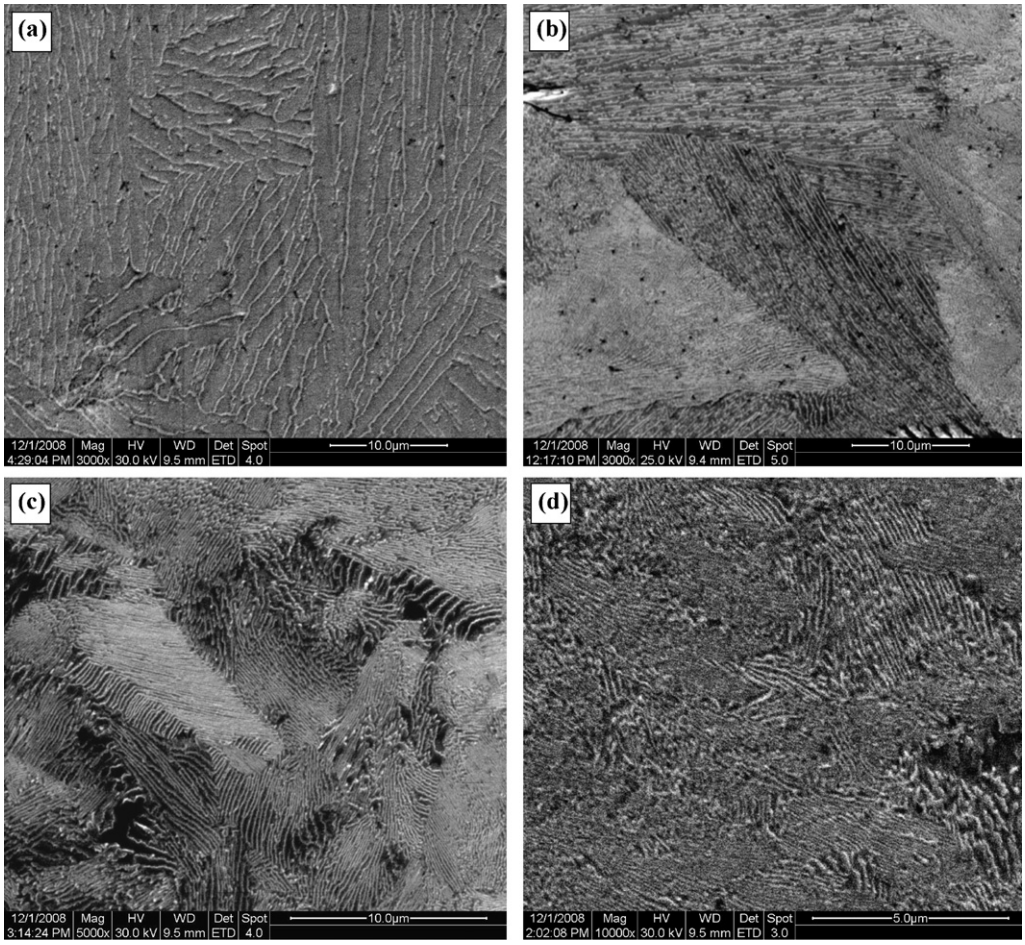

Fig. 3. Secondary electron images of as-cast U–Zr alloys; (a) U-2 wt%Zr, (a) U-5 wt%Zr, (c) U-7 wt%Zr and (d) U-10 wt%Zr. The inter-lamellar spacing reduces with increase in Zr content; also note the magnifications, (a) and (b) with 3000× (c) and (d) with 5000× and 10,000× respectively.

lower temperatures and that causes reduction in the inter-lamellar spacing.

Microhardness values of these alloys were obtained along with that of pure U. Total twelve nos. of measurements were taken. The plot of the average hardness vs. atom%Zr alongwith the standard deviation in the hardness values (shown as vertical bars) is presented in Fig. 4. The increase in hardness with Zr content could be attributed to the decreasing inter-lamellar spacing and the solution hardening effect. However, a tendency towards saturation in hardness is observed as Zr increases. Since, the inter-lamellar spacing depends on the Zr content; the hardness data can be fitted empirically as a function of Zr content alone:

$$H = H_U + 11.149X_{Zr} - 0.162X_{Zr}^2 \quad (1)$$

where, H_U is the measured hardness value of pure U, which is found to be 259.5 and X_{Zr} is the atom % of Zr.

3.2. XRD analysis

XRD results are presented in Fig. 5 for all the alloys. Clearly, all the alloys shows only α phase. It has already been established by Basak et al. that the α-U phase has a tendency to form supersaturated solution in U-2 wt%Zr alloy and $\gamma'' \rightarrow \alpha$ reaction is thermodynamically possible [5]. On the other hand, the peritectoid reaction ($\gamma''+\alpha \rightarrow \delta$) is extremely sluggish in nature and thus room temperature microstructure does not contain any delta phase. In fact Hills et al. has found that upto 20 at%Zr (~10 wt%Zr) only α-phase is present at room temperature [6]. So, from the prior knowledge combined with the XRD result and SEM micrograph; it is evident that during cooling the products of monotectoid reaction, i.e. β and γ'', transform into α phase keeping the lamellae intact; that is why at room temperature only supersaturated α phase is expected in all these U–Zr alloys.

Table 1
Typical chemical composition of U–Zr alloys.

Materials	Zr	U	C	N	O	Y	Fe	Ni	Cr	Mg	Mn	Ce
Uranium	–	Rest	252	32	188	105	64	15	11	16	8	6
Zirconium	Rest	–	27	10	227	12	120	60	44	10	–	–
Zr content and other impurities in the alloys												
U-2 wt%Zr	1.98% (5 at%)	Rest	316	40	532	120	77.5	33	16	14	9.8	4.1
U-5 wt%Zr	5.01% (12.1 at%)	Rest	354	42	544	168	62	29	14.5	8.4	8.5	–
U-7 wt%Zr	6.97% (16.4 at%)	Rest	371	65	571	182	80.5	35	5	7	–	2.2
U-10 wt%Zr	9.98% (22.4 at%)	Rest	450	60	580	204	40	25	4.8	16	5	8.7

Zr contents are in wt%; rest are in ppm. Additionally, zirconium contains Si and W less than 50 ppm each.

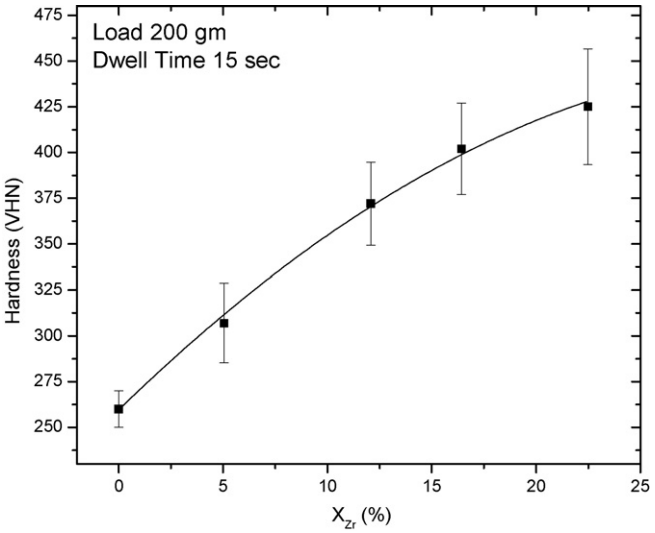

Fig. 4. Plot of the hardness vs. atom% Zr.

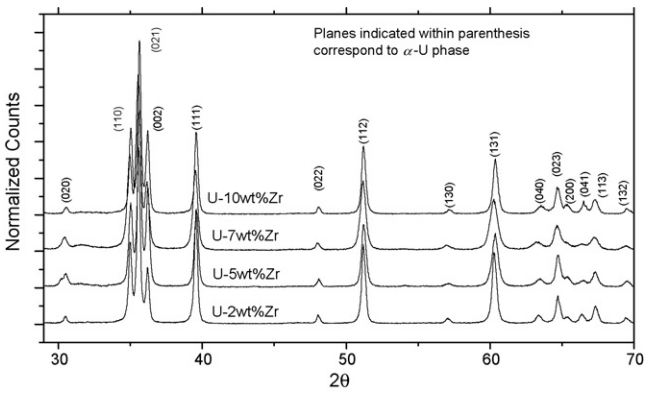

Fig. 5. Combined plot of XRD data of as-cast U–Zr alloys, note that all the peaks correspond to the α-U phase.

It is known that solute supersaturation changes the lattice parameters of the concerned phase. XRD data of all these as-cast alloys were subjected to the Rietveld analysis to compute the lattice parameters, using Powder Cell computer code [9]. The lattice parameter vs. Zr content (in atom%) are presented in Fig. 6(a–c) with a cubic fit; the equations are as follows:

$$a = a_0 + 4.3 \times 10^{-4} x_{Zr} - 2 \times 10^{-5} x_{Zr}^2 + 1.46 \times 10^{-7} x_{Zr}^3$$
$$b = b_0 - 3.8 \times 10^{-4} x_{Zr} + 2 \times 10^{-5} x_{Zr}^2 - 7.77 \times 10^{-7} x_{Zr}^3 \quad (2)$$
$$c = c_0 + 26.9 \times 10^{-4} x_{Zr} - 14 \times 10^{-5} x_{Zr}^2 + 2.54 \times 10^{-7} x_{Zr}^3$$

where a_0, b_0 and c_0 are the lattice parameters of the unalloyed uranium and are taken as 2.8536 Å, 5.8698 Å and 4.9555 Å respectively [10]. As evident from the Fig. 6(a–c); both a and c parameters increase towards some saturation values with increasing Zr content,

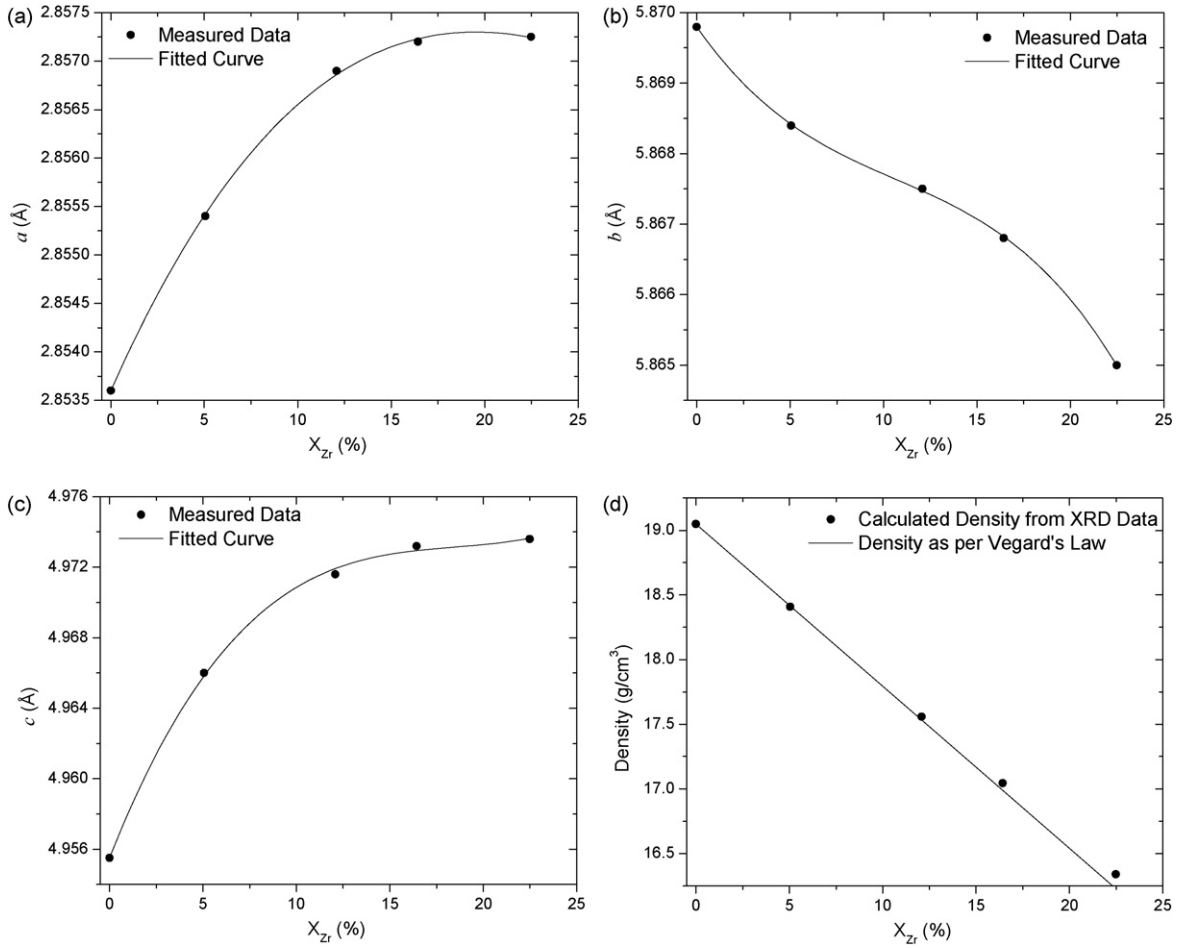

Fig. 6. (a–c) Variation in the lattice parameters in as-cast U–Zr alloys as a function of Zr content (atom%); (d) variation in bulk density of as-cast U–Zr alloys with Zr content.

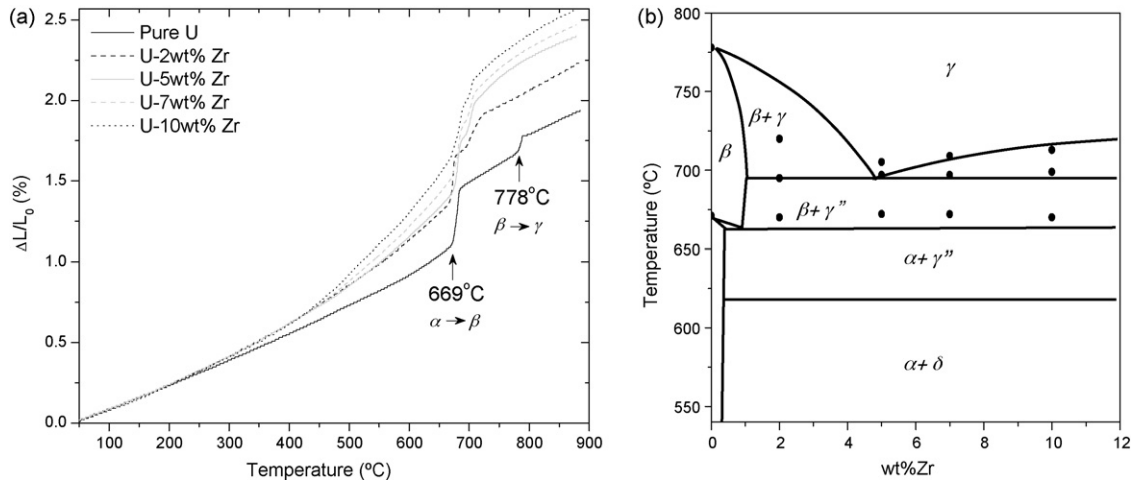

Fig. 7. (a) Thermal expansion curves for different U–Zr as-cast alloys, as obtained from the dilatometric experiments, with a heating rate of 1 °C/min. Note that the substantial increase in thermal expansion when 2 wt%Zr is added to uranium. (b) Phase transformation temperatures, derived from Fig. 6. (a), indicated by the black dots are superimposed on the U-rich part of the U–Zr phase diagram.

whereas *b* parameter decreases. The density was derived from the XRD analysis and is plotted in Fig. 6(d) as a function of Zr content along with the density calculated from the Vegards's law (i.e. considering α phase as an ideal solid solution of U and Zr). As expected the calculated density from XRD analysis deviates from the ideal solution behaviour as Zr increases.

3.3. Dilatometry

Dilatometry curves for all the as-cast alloys are presented in Fig. 7(a). As can be seen from the figure, thermal expansion increases drastically when pure U is compared to U-2 wt%Zr alloy (~5 at%Zr); however subsequent increase in Zr content has lesser influence on the thermal expansion.

From the dilatometric curves two distinct phase transformations are apparent; one slightly above 650 °C and another below 700 °C. The first transformation manifests a sharp change in length of the sample; however, the length change of the sample during the second transformation is gradual and hence it is possible to find the start and finish temperatures of the second transformation. All these phase transformation temperatures can be found out from the Fig. 7(a) and superimposed on the phase diagram of U–Zr; as presented in Fig. 7(b).

Metallographic results suggest presence of lamellar structure in these as-cast alloys, however, XRD analyses show the presence of α-phase only. So it can be concluded that there is uneven Zr distribution across the lamellar structure; in fact the earlier study on U-2 wt%Zr confirms the same [4]. Combining this information with Fig. 7(b) the following mechanism of phase transformation can be proposed; during heating the Zr-lean alpha phase undergoes α → β transformation above 670 °C (contrary to 662 °C of eutectoid temperature) and simultaneously Zr-rich alpha phase is transformed to γ″ directly. This temperature (~670 °C) thus does not correspond to the eutectoid point. As the temperature increases further, β and γ″ combine together and start forming γ phase (i.e. reverse of monotectoid reaction) at around 697 °C (compared to 693 °C of monotectoid reaction). Clearly this reaction is kinetically slow and gradual; that is why the change in length is not very sharp in the dilatometric curves. With increase in temperature more and more gamma phase forms. After some temperature, depending on the alloy composition, no more beta phase is available for the transformation and the sample contains only single phase gamma. Clearly, even with a slow heating rate of 1 °C/min. reverse of the eutectoid reaction was not observed, though the manifestation of the reverse monotectoid reaction is clear.

From the dilatometric curves it is possible to fit a cubic equation for the thermal expansion of the α-phase from 50 °C (323 K) to 650 °C (923 K), for different U–Zr alloys, as a function of temperature as follows:

$$\left(\frac{\Delta L}{L_0}\%\right)_{PureU} = -0.326 + 8.338\times10^{-4}T + 8.038\times10^{-7}T^2 - 1.465\times10^{-10}T^3$$
$$\left(\frac{\Delta L}{L_0}\%\right)_{2wt\%Zr} = -0.381 + 12.238\times10^{-4}T - 2.793\times10^{-7}T^2 + 9.904\times10^{-10}T^3$$
$$\left(\frac{\Delta L}{L_0}\%\right)_{5wt\%Zr} = -0.539 + 2.181\times10^{-3}T - 2.1\times10^{-6}T^2 + 2.087\times10^{-9}T^3 \quad (3)$$
$$\left(\frac{\Delta L}{L_0}\%\right)_{7wt\%Zr} = -0.62 + 2.732\times10^{-3}T - 3.386\times10^{-6}T^2 + 3.055\times10^{-9}T^3$$
$$\left(\frac{\Delta L}{L_0}\%\right)_{10wt\%Zr} = -0.73 + 3.489\times10^{-3}T - 5.154\times10^{-6}T^2 + 4.39\times10^{-9}T^3$$

where, temperature T is in K, L_0 is the initial length (at 50 °C) and ΔL is the difference between the instantaneous length (at any temperature T) and L_0. Higher Zr concentration and temperature both tend to form bcc gamma phase, as stated earlier; so with increase in Zr content cohesive energy is gradually reduced in orthorhombic crystal structure as temperature increases. This phenomenon manifests the increase in thermal expansion coefficient (slope of the dilatometric curves in α-phase region) of α-phase as Zr content increases in the alloys. However, it is important to note that the slopes of the dilatometric curves in γ-phase region for different Zr content do not vary much at same temperature; unlike the α-phase region.

As can be seen, expansion of γ phase increases with Zr content. The following equations are fitted for γ phase from 725 °C (998 K) to 900 °C (1173 K); however for pure *U*, the same was calculated from 790 °C (1063 K), i.e. well after β → γ transformation:

$$\left(\frac{\Delta L}{L_0}\%\right)_{PureU} = 81.794 - 21.986\times10^{-2}T + 19.985\times10^{-5}T^2 - 6.006\times10^{-8}T^3$$
$$\left(\frac{\Delta L}{L_0}\%\right)_{2wt\%Zr} = -7.775 + 2.405\times10^{-2}T - 2.105\times10^{-5}T^2 + 0.669\times10^{-8}T^3$$
$$\left(\frac{\Delta L}{L_0}\%\right)_{5wt\%Zr} = -55.041 + 14.778\times10^{-2}T - 12.804\times10^{-5}T^2 + 3.737\times10^{-8}T^3 \quad (4)$$
$$\left(\frac{\Delta L}{L_0}\%\right)_{7wt\%Zr} = -42.52 + 11.369\times10^{-2}T - 9.709\times10^{-5}T^2 + 2.804\times10^{-8}T^3$$
$$\left(\frac{\Delta L}{L_0}\%\right)_{10wt\%Zr} = -25.252 + 6.669\times10^{-2}T - 5.441\times10^{-5}T^2 + 1.518\times10^{-8}T^3$$

4. Conclusions

The present investigation, on the U-rich U–Zr alloys, provides microstructures, lattice parameter data and density as a function of Zr content; also thermal expansion equations are derived as a function of temperature. Besides these micrographs, data and equations presented here, the following inferences can be drawn with the help of combined interpretation of metallography, XRD analysis and dilatometry:

1. As cast grains of U–Zr alloys are irregular in shape and as Zr increases the average grain size reduces.
2. SEM micrographs show that the microstructures contain fine lamellae, fineness increases with Zr content in the alloys.
3. XRD analysis reveals that as-cast structure of all these alloys is single α-phase and density decreases with increase in Zr content.
4. The as-cast α-phases are supersaturated with Zr and deviates from the ideal solution behaviour as Zr increases.
5. Lattice parameter a and c, of these supersaturated α-phase, increase with Zr content; whereas, parameter b decreases; causing overall volume to increase.
6. These alloys undergo simultaneous $\alpha \rightarrow \beta$ and $\beta \rightarrow \gamma$transformation beyond 670 °C and reverse monotectoid reaction beyond 697 °C while heating; latter reaction is kinetically slow.

References

[1] L.C. Walters, J. Nucl. Mater. 270 (1999) 39–48.
[2] Y. Takahashi, M. Yamawaki, K. Yamamoto, J. Nucl. Mater. 154 (1988) 141–144.
[3] Y. Takahashi, K. Yamamoto, T. Ohsato, H. Shimada, T. Terai, M. Yamawaki, J. Nucl. Mater. 167 (1989) 147–151.
[4] G. Lagerberg, J. Nucl. Mater. 9 (1963) 261–276.
[5] C.B. Basak, R. Keswani, G.J. Prasad, H.S. Kamath, N. Prabhu, J. Alloys Compd., in press. doi:10.1016/j.jallcom.2008.04.021.
[6] R.F. Hills, B.R. Butcher, B.W. Howlett, J. Nucl. Mater. 16 (1965) 25–38.
[7] Report No. BMI-1030, Metallurgy and Ceramics (M-3679), 16th Ed., edited by F. A. Rough, Battelle Memorial Institute, 1955.
[8] Report No. BMI-1350, Metallurgy and Ceramics (TID-4500), 15th Ed., edited by A. A. Bauer, Battelle Memorial Institute, 1959.
[9] W. Kraus, G. Nolze, Bundesanstalt fuer Materialforschung und pruefung, Powder Cell v. 2.4, released on 08.03.2000.
[10] J.H. Lander, M.H. Mueller, Acta Crystallogr. B 26 (1970) 129.